JAERI-M
83-022

DROPLETS FLOW AND HEAT TRANSFER AT TOP REGION OF CORE IN REFLOOD PHASE

February 1983

Masahiro OSAKABE, Akira OHNUKI
and Makoto SOBAJIMA

日本原子力研究所
Japan Atomic Energy Research Institute

JAERI-Mレポートは，日本原子力研究所が不定期に公刊している研究報告書です。
入手の問合わせは，日本原子力研究所技術情報部情報資料課（〒319-11茨城県那珂郡東海村）あて，お申しこしください。なお，このほかに財団法人原子力弘済会資料センター（〒319-11茨城県那珂郡東海村日本原子力研究所内）で複写による実費頒布をおこなっております。

JAERI-M reports are issued irregularly.
Inquiries about availability of the reports should be addressed to Information Section, Division of Technical Information, Japan Atomic Energy Research Institute, Tokai-mura, Naka-gun, Ibaraki-ken 319-11, Japan.

編集兼発行　日本原子力研究所
印　　刷　㈱高野高速印刷

JAERI-M 83-022

Droplets Flow and Heat Transfer at Top Region of Core in Reflood Phase

Masahiro OSAKABE, Akira OHNUKI

and Makoto SOBAJIMA

Division of Nuclear Safety Research,
Tokai Research Establishment, JAERI

(Received January 28, 1983)

The heat transfer at the top region of core is complicated due to the strong thermal non-equilibrium just after the start of reflood phase in a postulated PWR-LOCA experiment. The film taken with a high-speed cinecamera shows upward droplets flow and falling water film on the non-heated rod just after the start of reflood at elevation 3235 mm above the bottom of heated length of heater rods in Slab Core Reflood Test. The measured mean diameter of droplet is about 1 mm. This value of mean diameter is larger than the measured result for the annular dispersed flow in a pipe. On the other hand, the corresponding Weber number is smaller than the Weber number in the accelerating flow obtained in the previous studies. The calculated heat transfer coefficient of the droplets flow approximately agrees with the sum of Dittus-Boelter's convective heat transfer term and radiative heat transfer term evaluated with the network analysis by Sun et al..

Keywords : PWR-LOCA, Reflood, Core, Droplet, Falling, Wated Film, Non-heated Rod, Diameter, Weber Number

再冠水過程における炉心上部での液滴流および熱伝達

日本原子力研究所東海研究所安全工学部
刑部　真弘・大貫　晃・傍島　真

（１９８３年１月２８日受理）

ＰＷＲ－ＬＯＣＡ時の再冠水過程開始直後における炉心上部の熱伝達は，強い熱的非平衡によって複雑なものとなっている。平板炉心再冠水試験で炉心発熱部下端から3,２３５mmの高さで，高速度シネカメラで得た写真は，再冠水開始直後に液滴上昇流と非加熱棒を伝わって流れ落ちる液膜を示していた。その液滴径を計測してみた結果，平均径は約1mmであった。この径は，単管内環状噴霧流で得られる値よりも大きい。一方，対応するウェーバー数は，加速流の中で従来得られているウェーバー数よりも少し小さい。その場所で求められた液滴流の熱伝達率は，Dittus－Boelter式で評価した対流項と，Sunらによるネットワーク解析で評価した放射伝熱項の和と，ほぼ一致した。

Contents

目　　次

1. Introduction

Slab Core Test Facility (SCTF) is a part of the Large Scale Reflood Test Program along with the Cylindrical Core Test Facility (CCTF) at the Japan Atomic Energy Research Institute (JAERI). One of the objectives of SCTF tests is to study the thermo-fluid dynamics in the core during the reflood phase in PWR-LOCA. Generally, the quench front goes upwards in the core. But the random quench at the top region of core can be observed. The heat transfer at the top region of core is complicated due to the strong thermal non-equilibrium and the effect of falling water film on the non-heated rod.

The observation result with the high-speed camera and the heat transfer coefficient at the top region of core in test S1-06 are introduced in this report. The major test conditions are shown in Table 1. The film taken with the high-speed camera shows the upward droplet flow at elevation 3235 mm from the bottom of heated length of heater rods. The droplets velocity and diameter are measured on the film. The heat transfer coefficient h [$W/(m^2 sK)$] defined by

$$h = q_w/(T_w - T_{sat}) \quad ,$$

where q_w : heat flux [$W/(m^2 \cdot s)$],
T_W : cladding temperature [K],
T_{sat} : saturation temperature [K],

is calculated near the view point. The correspondency of flow pattern and heat transfer coefficient is examined and discussed.

2. Observation with high-speed camera

2.1 High-speed camera system

High-speed camera is used to observe the flow pattern at the top region of core. The camera system has the following specifications.

(1) 16 mm high-speed cinecamera (photo-sonics 16-1PL)
- ○ Film length : 1200 ft
- ○ Film : 16 mm both-side perforation
- ○ Camera speed : 10 ∿ 500 frame per seconds (fPS), which can be changed in the operation.
- ○ Lens : Nikon 85 mm F2.0

(2) Camera controller
- ○ Camera speed can be changed with 24, 250 and 500 fPS by the remote-control.
- ○ The stop (f2.8 ∿ 22) can be changed automatically corresponding to the camera speed.

(3) Lighting system
- ○ Lamp : Xenon 300 W
- ○ Intensity of lighting: lighting flux ϕ100 mm and 8×10^4 Lux (at distance 1 m)

(4) Time recording system

The time display panel consists of LED (minimum displayed time is 1/1000 sec) can be taken to the lower part of the film frame by using the binary-photo system.

2.2 Observed location and error

Shown in Fig. 1 is the location of view-window in SCTF. In this study, the high-speed camera is set at the "Outlet of core" shown in Fig. 1. The elevation is 3235 mm from the bottom of heated length and 425 mm from the top of heated length. The schematic cross-section of SCTF is shown in Fig. 2. The view-window locates near the 6th

spacer from the bottom of heated length. The diameter of view-window is 43 mm.

The schematic diagram of observation with the high-speed camera is shown in Fig. 3. The lighting from opposite side window is used. The inside width of pressure vessel is 247 mm and the camera is set at 655.5 mm from the center of pressure vessel. In this configuration, the length ℓ_0, ℓ_1 and ℓ_2 shown in Fig. 3 are same on the film. This causes the error of measured length with the high-speed camera.

The obtained film is projected on the film motion analyzer and analyzed. The real dimension can be obtained from the diameter of window projected on the screen of motion analyzer. The diameter of window on the motion analyzer is ϕ163.65 mm and the real diameter is ϕ43 mm which corresponds to the length ℓ_2 in Fig. 3. If the length 43 mm is put at the center of pressure vessel, the corresponding length ℓ_2 becomes ℓ_2 = 51.1 mm from the geometric relation in Fig. 3. This ℓ_2 becomes 51.1 × 163.65/43 = 194.48 mm on the motion analyzer. The length 43 mm at the center line of pressure vessel is transformed on the motion analyzer with the following magnification factor M,

$$M = 194.48/43 \doteqdot 4.52.$$

The ratio e of real to measured length in the observed space is within,

$$\frac{\ell_1}{\ell_0} \leq e \leq \frac{\ell_2}{\ell_0} \quad (0.81 \leq e \leq 1.2) \quad , \tag{1}$$

with the geometric relation in Fig. 3. The ratio described with Eq.(1) is applicable when the diameter of droplets is measured on the film. In this study, the error of measured droplet diameter is within ±20 % from Eq.(1).

When the velocity is measured with the trace of droplets, the error is much more complicated. In Fig. 4 the trace of droplets is shown as a vector. As the real dimension on the film is obtained by the dimension on the center line of pressure vessel, the trace in the Z-direction becomes Z' on the film. The error E in this measurement is written as,

$$E = \frac{Z' - (Z + \Delta Z)}{Z + \Delta Z} \times 100 \tag{2}$$

By the geometric relation in Fig. 4,

$$\frac{E}{100} = (1 - \tan\theta \cdot \tan\varphi) \frac{L}{x+L} - 1 . \qquad (3)$$

Equation (3) shows the error when the velocity in the Z-direction is measured with the camera. The maximum error using Eq.(3) is calculated in the observed space as follows. The droplets observed in this study are moving upwards with high speed. The vector is considered within $-\pi/6 \leq \theta \leq \pi/6$. The maximum error in the observed space is calculated by using Eq.(3). When the angle θ is within $-\pi/6 \leq \theta \leq \pi/6$,

$$|E|_{max.} = 27.9\ \% .$$

2.3 General observation results

Shown in Photo. 1 through Photo. 4 are the examples of transient flow patterns. The shutter speed is 5×10^{-5} s . The two rows of electric heater rods can be seen in the photographs. A non-heated rod is included in the right row. The diameters of heated and non-heated rods are 10.7 and 13.8 mm, respectively. The number of rods in the depth direction is 16. Just after the start of reflood (time = 0 s), high speed small droplets are moving up and the amount of droplets is increasing. Shown in Fig. 5 is the void fraction at bundles 2 and 4 obtained from the differential pressure between elevation 3235 and 2695 mm neglecting the frictional loss.It is noticed that the underestimation of void fraction due to the frictional loss is included at the first period in Fig. 5. The decreasing void fraction corresponds to the increasing amount of droplets observed on the film. Shown in Fig. 6 is the cladding temperature of non-heated rod at the view point. At elevation 3620 and 2760 mm from the bottom of heated length, the non-heated rod is quenched in 5 and 9 s , respectively. After this time, the wavy water film on the non-heated rod can be seen on the film.

3. Results and discussions

3.1 Diameter and velocity of droplet

Shown in Fig. 7 are the measured diameters of droplets versus time with the arbitrary sampling. The diameter of droplet is the average in the horizontal and vertical directions. The mean diameter is $\bar{d} \simeq 1$ mm. The lines shown in Fig. 8 are the superficial steam velocities obtained from the steam mass flow rates measured with Venturi flow meter after steam/water separator at the outlet of core and the assumed steam temperaure T_g [K]. The steam temperature T_g in the core is assumed as,

$$T_g = T_{sat} + \left(\frac{T_w - T_{sat}}{2} \right) \frac{\eta}{100} \quad . \tag{4}$$

The cladding temperature T_w at elevation 3190 mm near the view point is used to evaluate the steam temperature T_g in Eq.(4). The cladding temperature of elevation 3190 mm in bundle 3 is about 700 K between 0 and 20 s after the start of reflood. The parameter of superheat η is assumed as 150, 100, 50 and 0 % in Fig. 8. η = 150 % corresponds to the superheat of about 250 K in this study. The steam generation above the measured elevation 3235 mm is smaller than that below 3235 mm and neglected. The circles (○) and triangles (△) in Fig. 8 are the superficial steam velocity obtained from the droplet velocity by the following manner. As the steam velocity u_g is nearly equal to the superficial steam velocity U_g in the droplet flow, U_g is expressed as

$$U_g \simeq u_g = \left(\frac{4 \cdot \Delta\rho \cdot g \cdot d}{C_D \cdot 3\rho_g} \right)^{1/2} + u_d \quad , \tag{5}$$

where
- C_D : drag coefficient,
- g : acceleration due to gravity [m/s^2],
- $\Delta\rho$: $\rho_\ell - \rho_g$ [kg/m^3] ,
- d : droplet diameter [m] ,
- u_d : droplet velocity [m/s] ,
- ρ_g : density of steam [kg/m^3] ,
- ρ_ℓ : density of water [kg/m^3] .

The velocity of droplet, which diameter is lager than 1 mm, is measured. The measured velocity and diameter of droplet are substituted in Eq. (5). The drag coefficients C_D are assumed as 0.45 (circles ○) and 1.0 (triangles △). The upper and lower limits in data are obtained with

the steam superheat of 300 and 0 K, respectively in Eq.(5). The standard drag curve[1] of rigid sphere shows $C_D = 1.0 \sim 0.45$ in the range of particle Reynolds number $Re_p = 10^2 \sim 10^3$ which covers the range of this study.

The evaporation of droplets reduces the drag coefficient due to mass flux from the surface. Bailey et al.[2] suggested the ratio of drag coefficient C_{DO} with evaporation and C_D with no evaporation as,

$$C_{DO}/C_D = 1/(1 + B) \quad , \tag{6}$$

where $B = C_g \frac{\Delta T_{sat}}{H_{fg}}$ (Spalding number) ,

C_g : specific heat of vapor [J/(kg·K)] ,

ΔT_{sat} : vapor superheat [K] ,

H_{fg} : latent heat of evaporation [J/kg].

As the maximum superheat of vapor in this study is considered as 300 K, the minimum ratio of Eq.(6) is

$$C_{DO}/C_D = 0.78 \ .$$

The circulation of liquid inside the moving drop has been studied and summarized by Hidy and Brock[3]. They proposed the ratio of C_{DO} with circulation and C_D with no circulation as,

$$C_{DO}/C_D = \frac{1 + 0.75(\mu_g/\mu_\ell)}{1 + (\mu_g/\mu_\ell)} \quad , \tag{7}$$

where μ_g, μ_ℓ : dynamic viscosity of gas and liquid (Pa·s) .

In this study of SCTF,

$$C_{DO}/C_D \doteq 1.0 \quad .$$

The evaporation of droplets reduces the drag coefficient. However, the drag coefficient $C_D = 0.45 \sim 1.0$ is enough to cover the experimental range in this study. The velocities assuming $C_D = 0.45$ or 1.0 in Eq.(5) are larger than the measured result evaluated with $\eta = 150$ % between 2 and 10 s and agree with it between 10 and 15 s in Fig. 8.

Ueda[4] proposed the following correlation for the mean droplets diameter observed at air-water annular dispersed flow in a pipe.

$$\frac{d_m}{D} = 5.8 \times 10^{-3} \left[\frac{\sigma}{\mu_g U_g} \left(\frac{\rho_g}{\rho_\ell} \right)^{1.25} \right]^{0.34} , \tag{8}$$

where, d_m : mean diameter defined by $\sqrt{\Sigma d^3/\Sigma d}$ (m) ,
σ : surface tension (N/m) ,
μ_g : dynamic viscosity of gas (Pa·S) ,
U_g : superficial velocity of gas (m/s) ,
ρ_g : gas density (Kg/m^3) ,
ρ_ℓ : liquid density (Kg/m^3) ,
D : diameter of pipe (m).

The mean diameter d_m is evaluated as $(4\sim2)\times10^{-2}$ mm with Eq.(8)by using the superficial steam velocity 5∿15 m/s based on Fig.8, the steam superheat 0∿ 300 K and the equivalent diameter of the subchannel as a pipe diameter D. This value of mean droplet diameter is much smaller than the present result $\bar{d} \simeq 1$ mm. This suggests that the different mechanism is dominant to make the entrained droplets from that of annular flow described by Eq. (8). On the other hand, the Weber number is defined as,

$$We = \rho_g (u_g - u_d)^2 \bar{d}/\sigma , \tag{9}$$

where u_g : steam velocity (m/s),
u_d : droplet velocity (m/s),
$\bar{d}$: mean droplet diameter (m) .

From Eqs. (5) and (9),

$$We = \left(\frac{4 \cdot \Delta\rho \cdot g \cdot \bar{d}}{C_D \cdot 3\rho_g} \right) \rho_g \cdot \bar{d}/\sigma . \tag{10}$$

The minimum value of drag coefficient is considered to be $C_D = 0.45$ in this study. By substitution of $\bar{d} = 1$ mm and $C_D \geq 0.45$ into Eq.(10),

$$We \leq 0.5 .$$

Ishiki[5] proposed that We = 6.5 agreed with his measured water droplet diameters which were breaking up in accelerating flow. Forsulund et al.[6] proposed We = 7.5 for liquid nitrogen drop in the accelerating

vapor stream. The Weber number in this study is smaller than their Weber number. This means the smaller droplet diameter than their results.

3.2 Heat transfer coefficient of droplet flow

Shown in Figs. 9 and 10 are the measured heat transfer coefficients at elevation 3190 mm (circles o: adjacent to non-heated rod, triangles Δ: not adjacent to non-heated rod). A little higher heat transfer coefficient adjacent to non-heated rod is obtained than that not adjacent to non-heated rod. The referred lines are calculated with,

$$h = h_{con} \cdot (T_w - T_g)/(T_w - T_{sat}) + h_{rad} \quad , \tag{11}$$

where $h_{con} = 0.023 \frac{\lambda_g}{D_e} Re^{0.8} Pr^{0.4}$ (Dittus-Boelter) ,

λ_g : Thermal conductivity of steam [w/(m·K)] ,
D_e : Equivalent diameter of subchannel [m] ,
Re : Reynolds number ($= U_g \cdot D_e/\nu_g$) ,
U_g : Superficial steam velocity [m/s] ,
ν_g : Kinematic viscosity of steam [m^2/s] ,
Pr : Prandtl number of steam .

The cladding temperature adjacent to non-heated rod is used as T_w in Eq.(11). The physical properties are evaluated with the film temperature $(T_w + T_g)/2$. h_{rad} is radiation heat transfer coefficient defined with,

$$h_{rad} = [F_{w\ell} \cdot E \cdot (T_w^4 - T_{sat}^4) + F_{wv} \cdot E \cdot (T_w^4 - T_g^4)]/(T_w - T_{sat}),$$

where E : Stefan-Boltzmann constant [$W/(m^2 \cdot K^4)$],
$F_{w\ell}, F_{wv}$: gray body factor .

The first term expresses the radiative heat transfer from cladding to droplets and the second expresses that from cladding to steam. The values of $F_{w\ell}$ and F_{wv} are obtained with Sun et al.'s[7] network analysis assuming the droplet flow as gray and diffuse. $F_{w\ell}$ and F_{wv} are the function of void fraction, mean droplet diameter and the steam superheat. In this study, the mean droplet diameter $\bar{d}$ is assumed as 1 mm. Figure 9

shows the effect of superheat. The higher superheat decreases the heat transfer coefficient. In this figure, the void fraction is assumed as $\alpha = 0.9$. The effect of void fraction assuming $\eta = 150$ % is shown in Fig. 10. As the cladding temperature T_w not adjacent to non-heated rod is almost the same with that adjacent to non-heated rod between 0 and 20 s after the start of reflood, Eq.(11) using T_w adjacent to non-heated rod is applicable for the data not adjacent to non-heated rod. Between 10 and 20 s, the actual void fraction α is lager than 0.96 considering the underestimation due to the frictional loss in Fig. 5 and the superheat η = 150 % is appropriate in Fig.8. The heat transfer of droplets flow approximately agrees with Eq.(11) by using the superheat η = 150 % and the void fraction $\alpha = 0.9 \sim 0.999$ between 10 and 20 s in Fig. 10.

4. Conclusions

1. The droplet diameter and velocity are measured at the top region of core. The measured mean diameter of droplets is $\bar{d} \simeq 1$ mm. This value is much larger than the entrained droplet from annular flow in a pipe.
2. Weber number in this study is considered to be less than 0.5. This value is smaller than the Weber number in the accelerating flow proposed by Ishiki and Forsulund et al..
3. The heat transfer coefficient of droplet flow approximately agrees with the sum of Dittus-Boelter's convection term and radiative heat transfer term by Sun et al..

Acknowledgement

The authors are much indebted to Drs. S. Katsuragi and M. Ishikawa, Head and Deputy Head of Div. Nuclear Safety Research, respectively. They would like to express their appreciation to Dr. K. Hirano, Mr. H. Adachi, Dr. Y. Murao, Dr.Y.Sudo and Mr. T. Iwamura for their useful discussions.

References

1. Clift, R., et al.: "Bubbles, Drops and Particles", Academic Press, (1978)
2. Bailey, G.H., et al.: Brit. Chem. Eng., Vol. 15, No. 7, 912 (1970)
3. Hidy, G.M., et al.: The Dynamics of Aerocolloidal System, Pergamon Press, (1970)
4. Ueda, T.: NIHON-KIKAI-GAKKAI RONBUN-SHU (Trans. Japan Soc. Mech. Engrs.), 45-389, (1970), (in Japanese)
5. Ishiki, M.: Report No. 35, Transportation Technical Research Institute, Tokyo, Japan (1959)
6. Forsulund, R.P., et al.: J. of Heat Transfer, 399, (1968)
7. Sun, K.H., et al.: J. of Heat Transfer, 414, (1976)

Table 1 Test condition

Test No.	S1-06
Test type	Forced flooding
System pressure	0.2 MPa
Core inlet velocity Acc* for ∿10 s LPCI** after Acc	 5 cm/s 2.5 cm/s
Max. core inlet subcooling	17.8 K
Max.cladding temperature at start of reflood	970 K
Power	1.2 ANS + Actinides + Delayed neutron fission with void feed back

* Accumulator injection
** Low pressure coolant injection

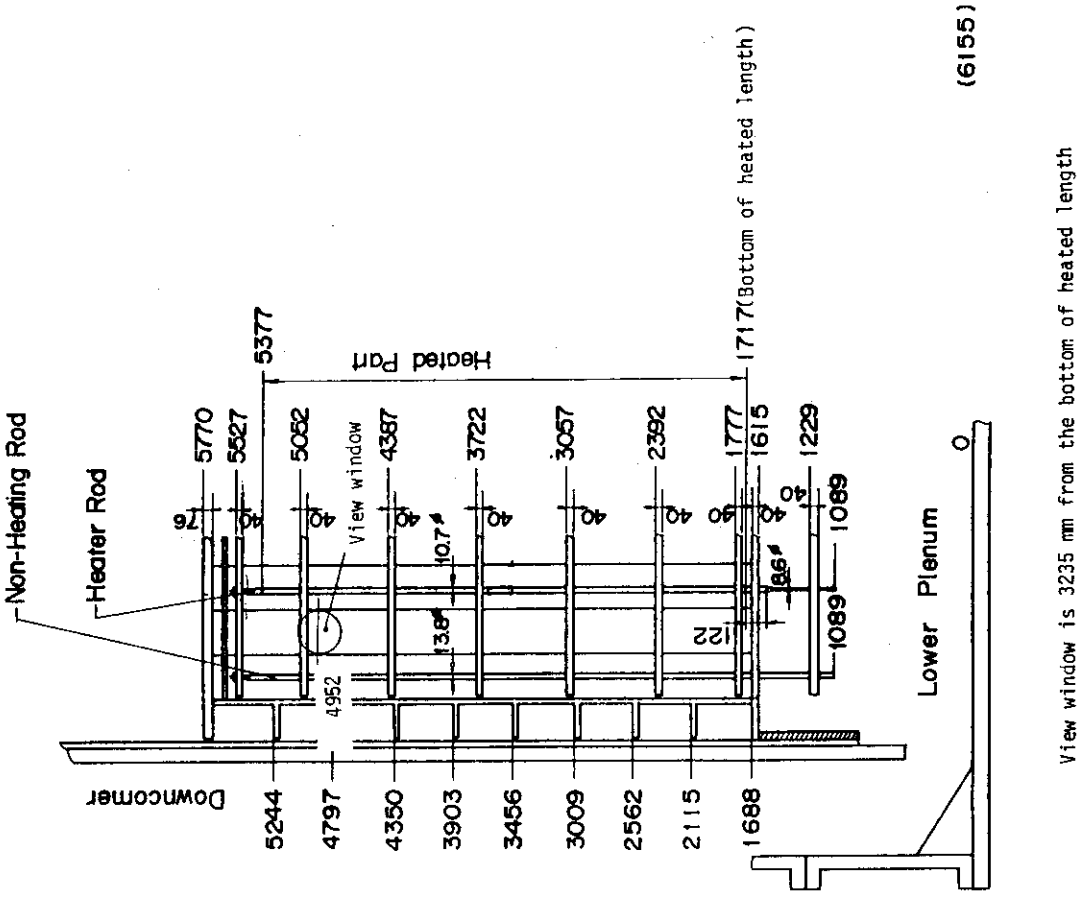

Fig. 2 Schematic cross-section of SCTF

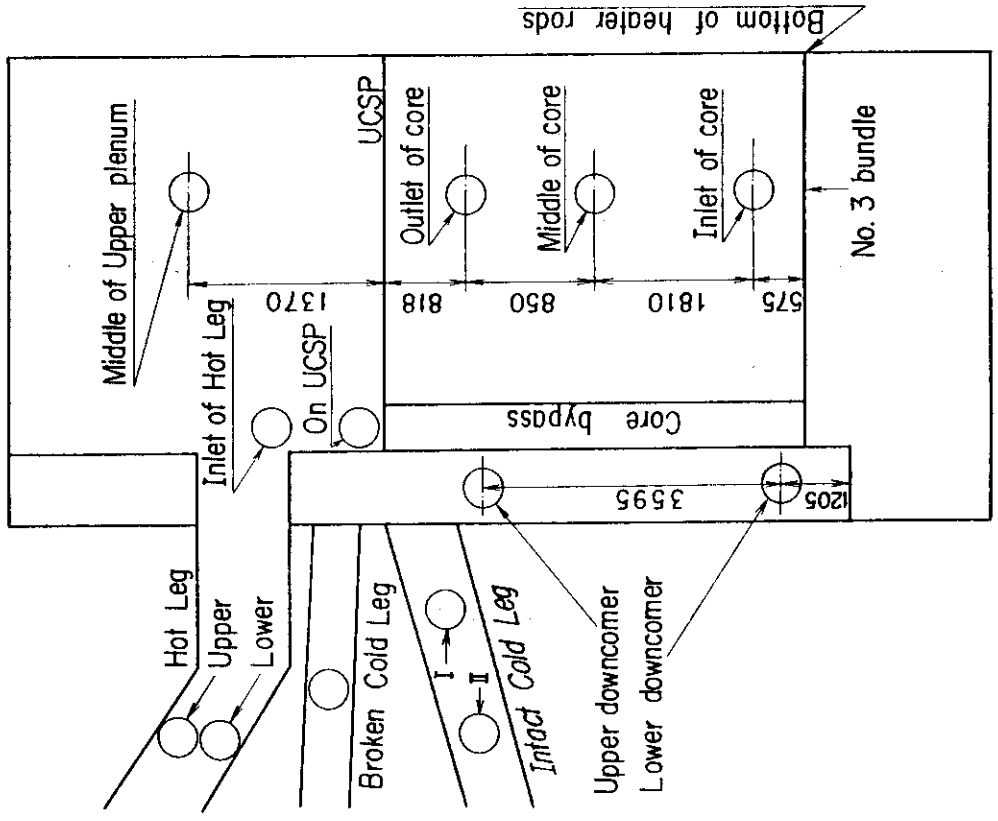

Fig. 1 Location of view-window in SCTF

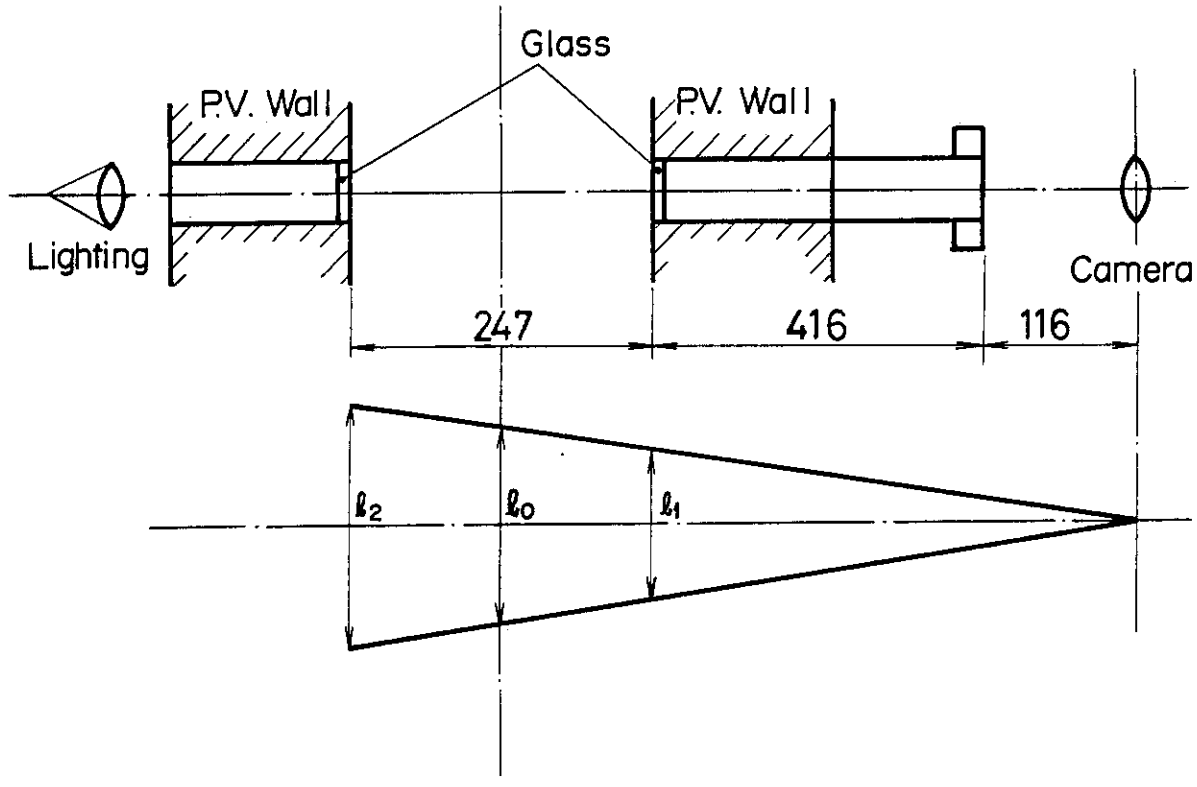

Fig. 3 Schematic diagram of observation with high-speed camera

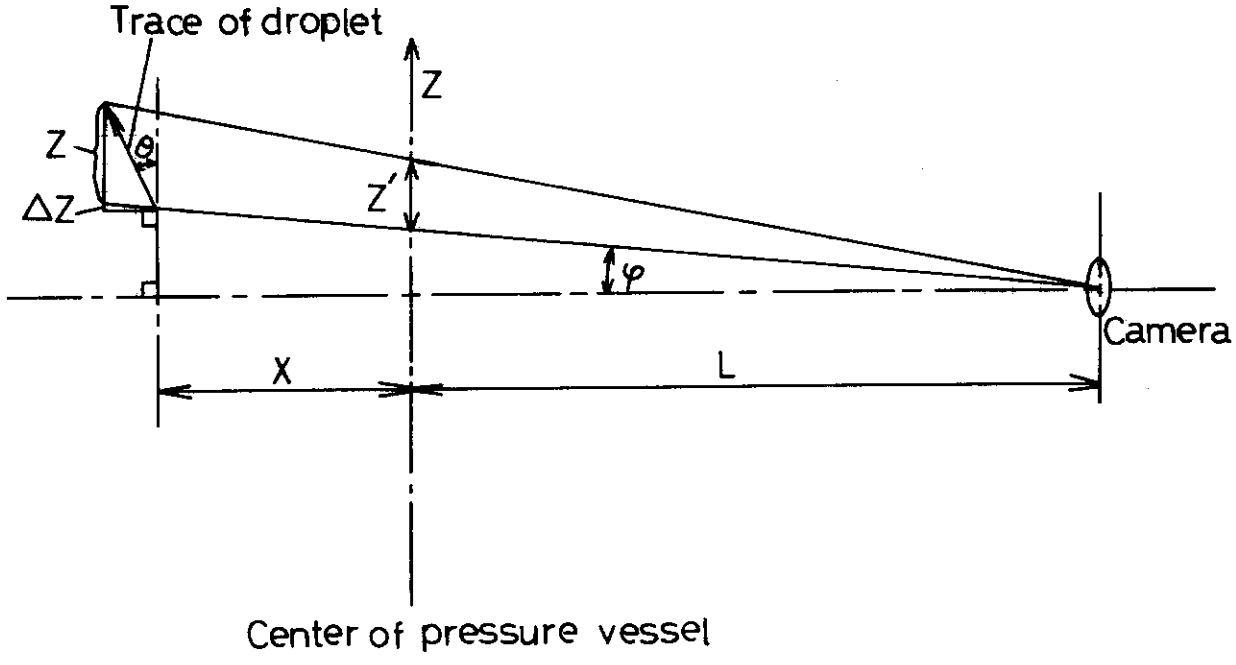

Fig. 4 Trace of droplets observed with high-speed camera

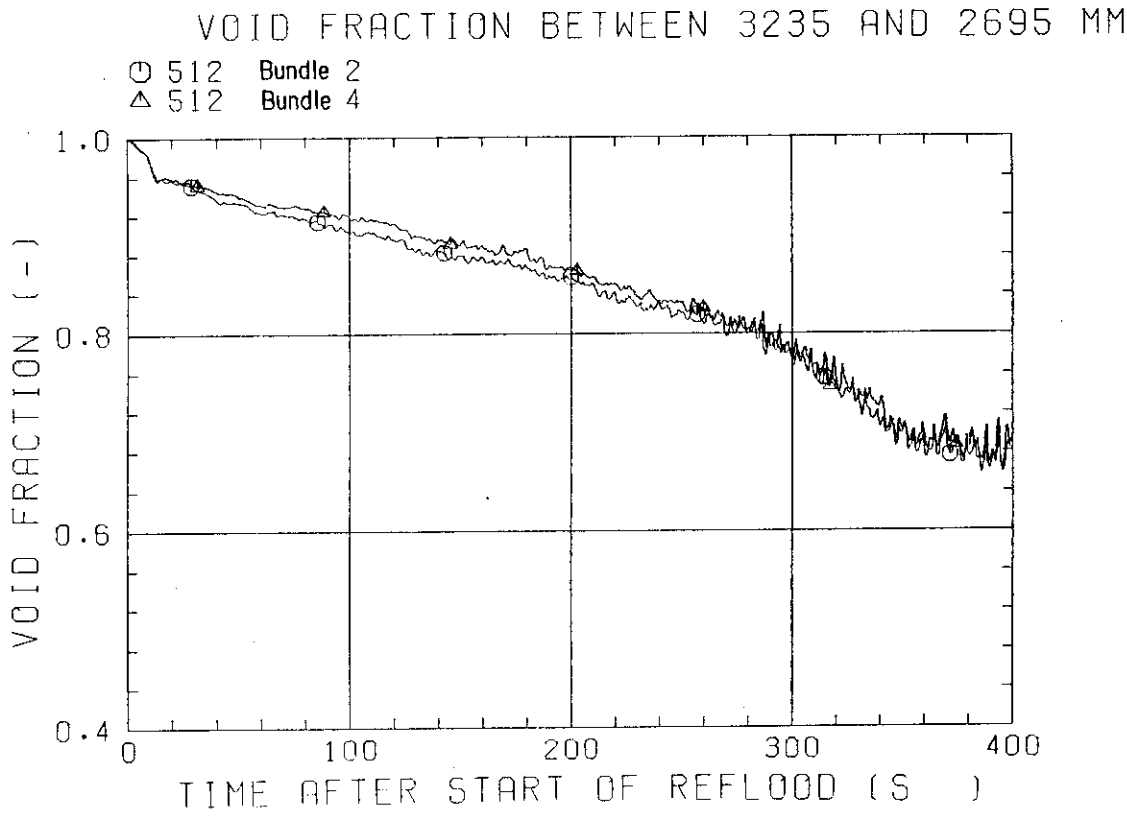

Fig. 5 Void fraction measured between 3235 and 2695 mm from the bottom of heated length.

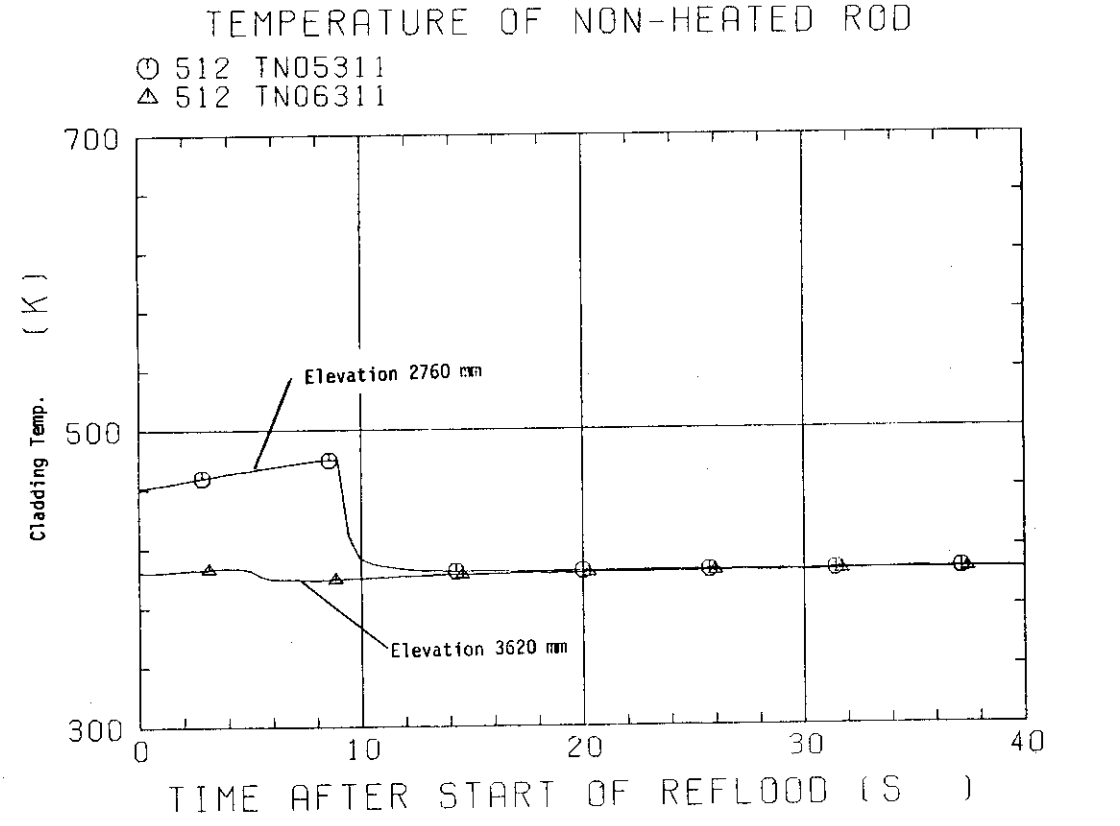

Fig. 6 Cladding temperature of non-heated rod at the view-point

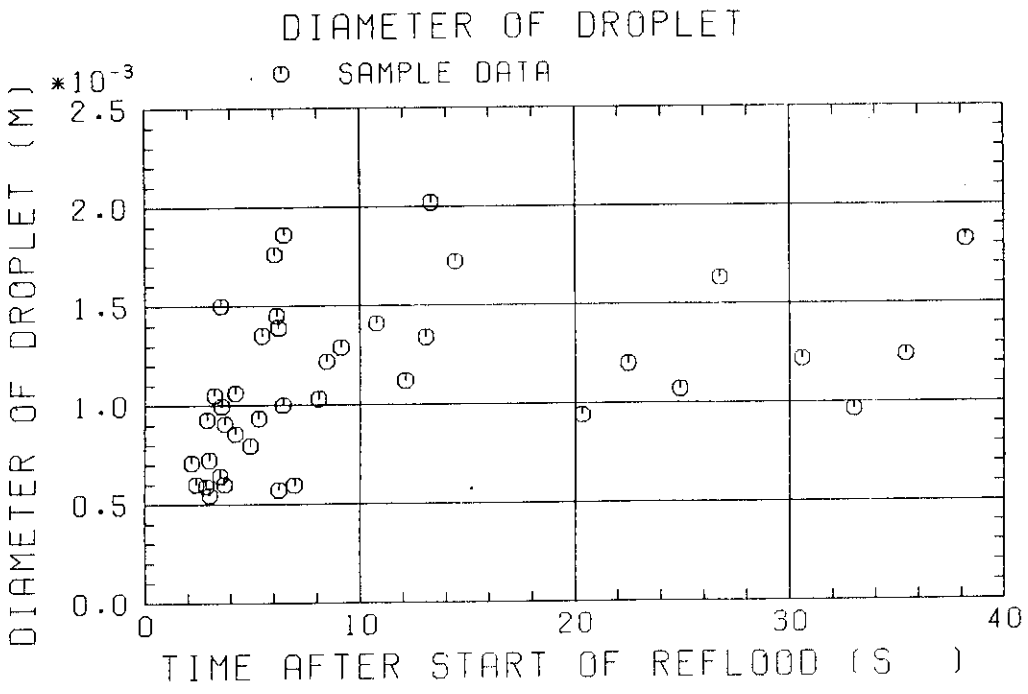

Fig. 7 Droplet diameters

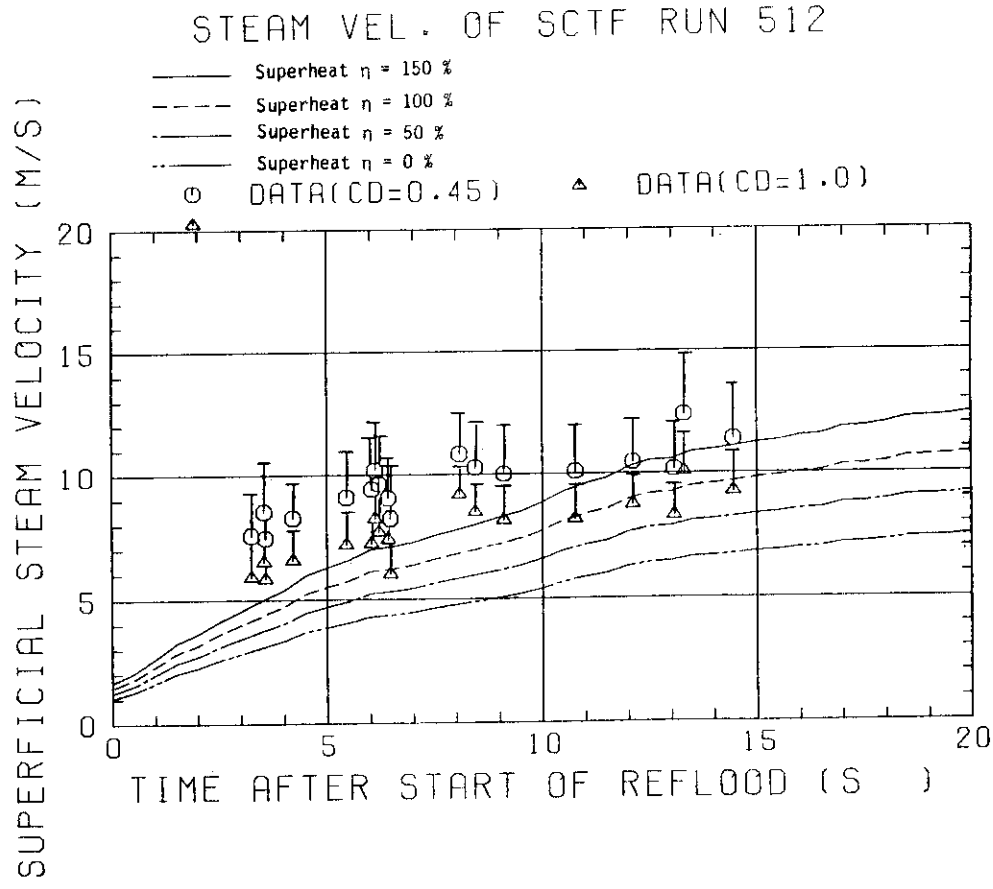

Fig. 8 Superficial steam velocity

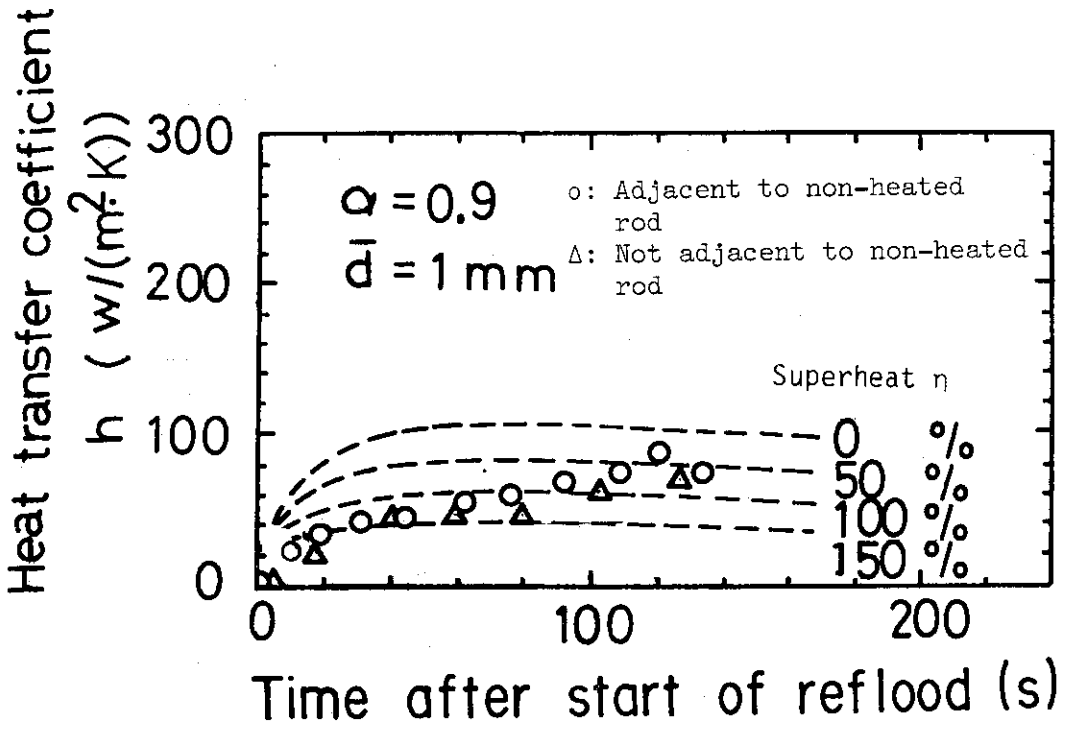

Fig. 9 Effect of vapor superheat on heat transfer coefficient

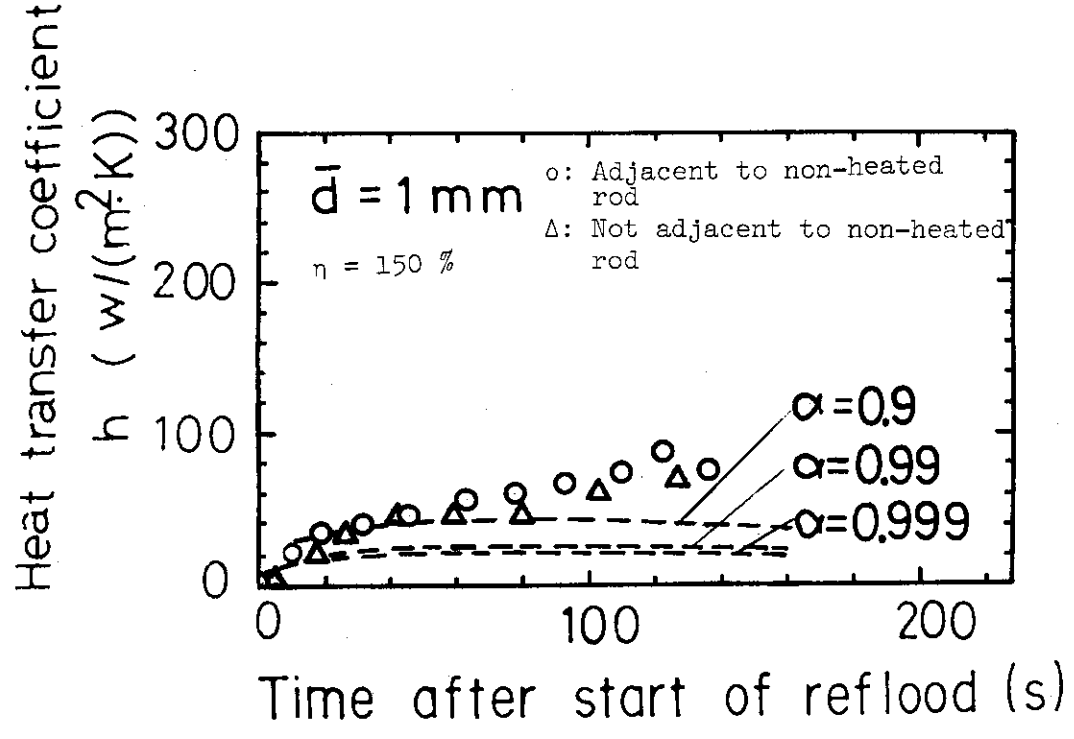

Fig. 10 Effect of void fraction on heat transfer coefficient

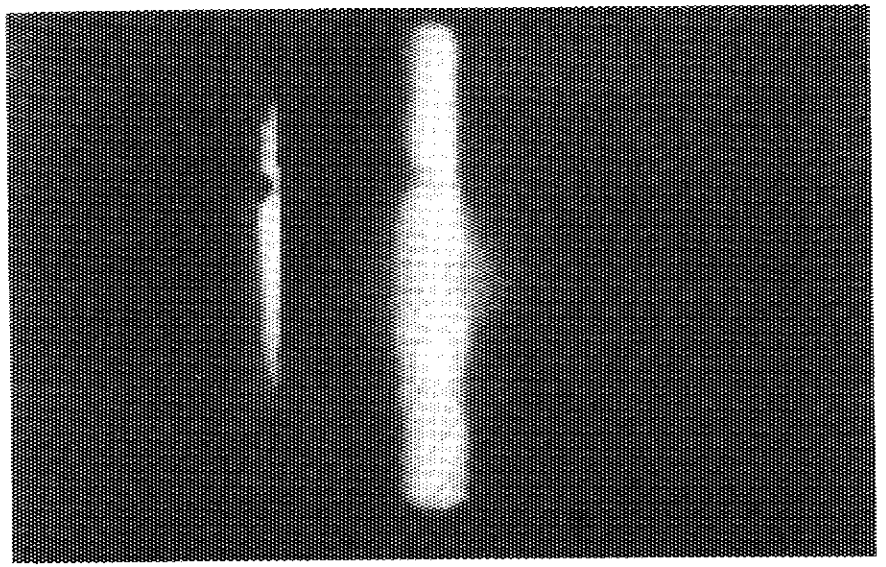

Photo.1 Time = 91.969 s (5.969 s from start of reflood).

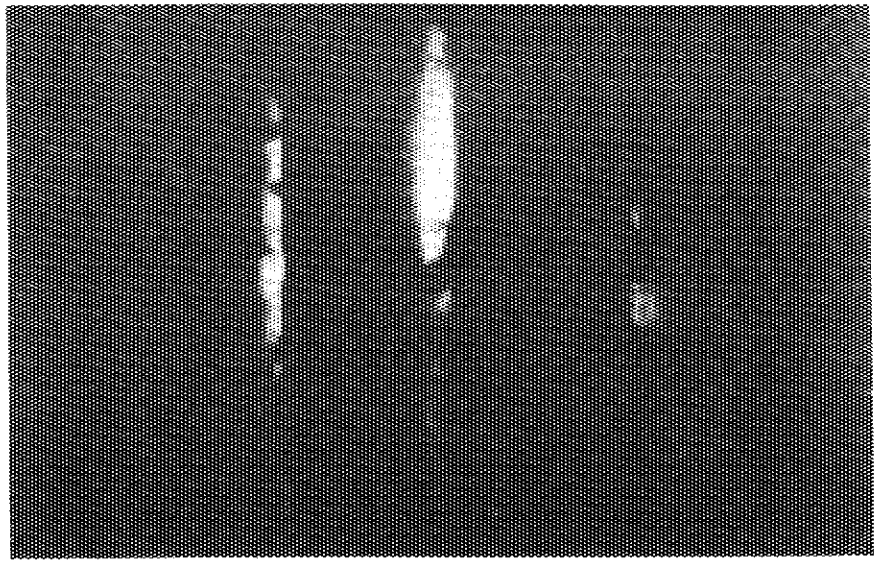

Photo.3 Time = 103.997 s (17.997 s from start of reflood).

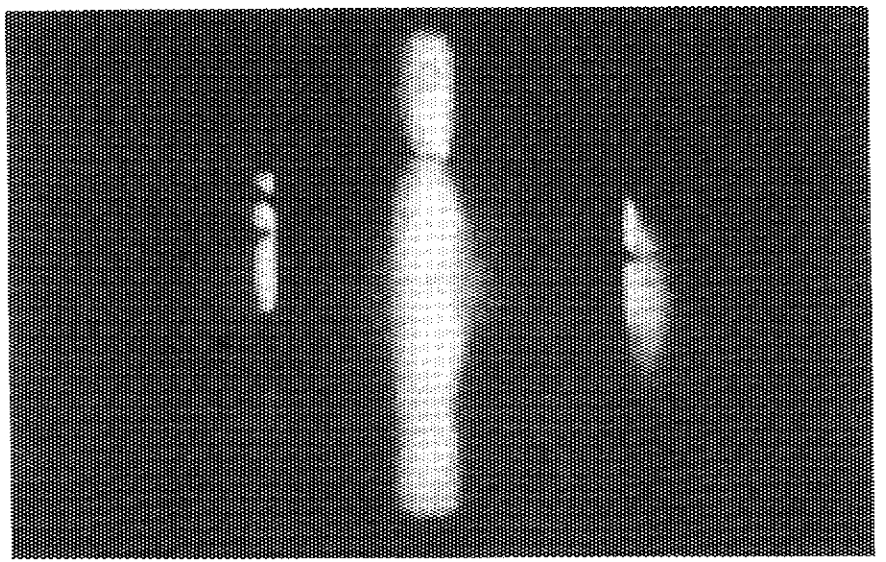

Photo.2 Time = 93.014 s (7.014 s from start of reflood).

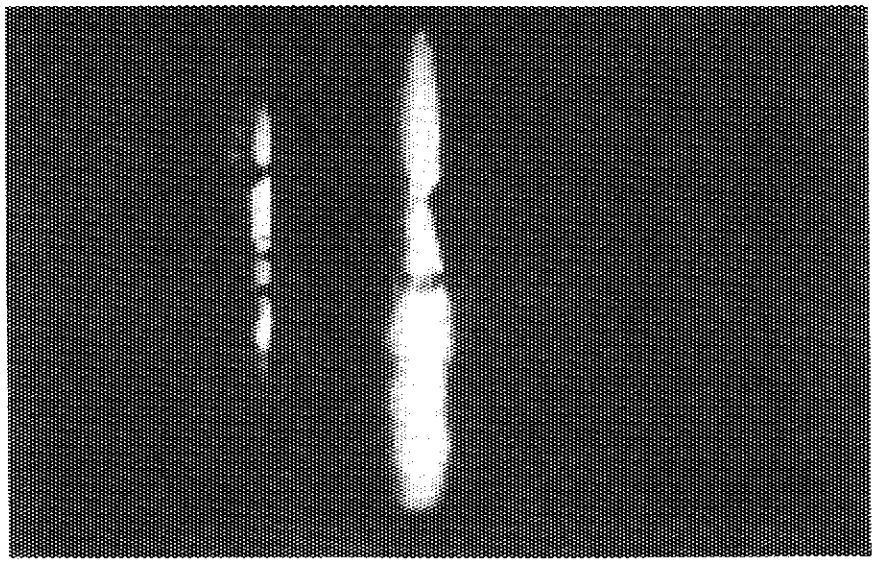

Photo.4 Time = 105.129 s (19.129 s from start of reflood).

Appendix Schematic of Slab Core Test Facility (SCTF)

A.1 Test facility

The Slab Core Test Facility (SCTF) is designed under the following design philosophy and design criteria.

(1) The reference reactor for simulation to the SCTF is the Trojan reactor in the United States which is a four loop 3300 MWt PWR. The Ooi etc. in Japan are also referred which are similar types to the Trojan reactor.

(2) A full scale radial and axial section of a pressurized water reactor is provided as a simulated core of the SCTF with single bundle width.

(3) The simulated core consists of 8 bundles arranged in a row. Each bundle has electrically heated rods simulating fuel rods and non-heated rods simulating control rods.

(4) The flow area and fluid volume of components are scaled down based on the core flow area scaling.

(5) The honeycomb structure is used as the side wall to minimize the effect of wall on the core thermo-hydrodynamics.

(6) The facility is provided with a hot leg (equivalent to four actual legs) connecting the upper plenum and the steam/water separator, an intact cold leg (equivalent to three actual intact cold legs) connecting the steam/water separator and the downcomer and two broken cold legs (one for the steam/water separator side, the other for the downcomer side).

(7) The ECCS consists of Acc, LPCI and a combined injection system.

The overal schematic diagram of the SCTF is shown in Fig. A-1. The principal dimensions of the SCTF are shown in Table A-1. The comparison of dimensions between the SCTF and the referred PWR is shown in Fig. A-2. The heights of the component in the pressure vessel are almost the same as the reference reactor's.

A.1.1 Pressure Vessel and Internals

The pressure vessel is of slab geometry as shown in Fig. A-3. The core consists of 8 bundles in a row and each bundle includes simulated fuel rods and non-heated rods with 16×16 array. The core is surrounded with the honeycomb thermal insulator which is attached on the barrel. The downcomer is located at one end of the pressure vessel

which corresponds to the periphery of the actual PWR. The core baffle region is located between the core and the downcomer.

The design of upper plenum internals is based on that of the new Westinghouse 17×17 array fuel assemblies. The radius of each internal is scaled down by factor 8/15 of an actual reactor.

The heights of the hot leg and cold legs are designed as close to the actual PWR as possible. However, the heights of nozzles for the broken cold leg and the intact cold leg are shifted down compared to that of the hot leg in order to avoid the interference of nozzles in downcomer as shown in Fig. A-3.

A.1.2 Heater Rod Assembly

The heater rod assembly for the SCTF core-I consists of 8 bundles arranged in a row. Each bundle has 234 electrically heated rods and 22 non-heated rods. The dimensions of heater rods are based on a 15×15 fuel rod bundle, and the heated length and the outer diameter of each heater rod are 3.66 m and 10.7 mm, respectively. The heater rods consist of a nichrome heater element, magnesium oxide (MgO) and Nichrofer-7216 sheath (equivalent to Inconel 600). The sheath wall thickness is about 1.0 mm and is thicker than the actual fuel cladding for the thermocouple installation. The heater rods don't simulate the gap conductance which is a feature of actual fuel rod. The axial peaking factor of rods power is 1.4.

A.1.3 Primary Loops and ECCS

Primary loops consist of a hot leg, a steam/water separator for measuring the flow rate of carry-over water, an intact cold leg, two broken cold legs. Two broken cold legs are connected with two containment tanks through break valves. A pump simulator and a loop seal part are provided for the intact cold leg. The pump simulator consists of the casing and duct simulators and an orifice plate to simulate the flow resistance.

ECCS consists of an accumulator and a low pressure injection system. The injection port for the forced reflooding test is at the lower plenum.

A.1.4 Containment Tanks and Auxiliary System

Two containment tanks are provided to the SCTF. The containment tank-I is connected to the downcomer with the pressure vessel side

broken cold leg. The containment tank-II is connected to the steam/water separator with the steam/water separator side broken cold leg.

A.2 Instrumentation

The instrumentation in the SCTF has been provided both by JAERI and the USNRC. The JAERI-provided instrumentation includes the measurement of temperatures, pressures, differential pressures, liquid levels, flow velocities, and heating powers. The USNRC has provided film probes, impedance probes, string probes, liquid level detectors (LLDs), fluid distribution grids (FDGs), turbine meters, drag disk, γ-densitometers, spool pieces and video optical probes.

Table A-1 Principal Dimensions of Test Facility

1. Core Dimension		
(1) Quantity of Bundle	8	Bundles
(2) Bundle Array	1×8	
(3) Bundle Pitch	230	mm
(4) Rod Array in a Bundle	16×16	
(5) Rod Pitch in a Bundle	14.3	mm
(6) Quantity of Heater Rod in a Bundle	234	rods
(7) Quantity of Non-Heated Rod in a Bundle	22	rods
(8) Total Quantity of Heater Rods	234×8=1872	rods
(9) Total Quantity of Non-Heated Rods	22×8=176	rods
(10) Effective Heated Length of Heater Rod	3660	mm
(11) Diameter of Heater Rod	10.7	mm
(12) Diameter of Non-Heated Rod	13.8	mm
2. Flow Area & Fluid Volume		
(1) Core Flow Area* (nominal)	0.227	m^2
(2) Core Fluid Volume	0.92	m^3
(3) Baffle Region Flow Area	0.10	m^2
(4) Baffle Region Fluid Volume	0.36	m^3
(5) Downcomer Flow Area	0.121	m^2
(6) Upper Annulus Flow Area	0.158	m^2
(7) Upper Plenum Horizontal Flow Area	0.525	m^2
(8) Upper Plenum Fluid Volume	1.16	m^3
(9) Upper Head Fluid Volume	0.86	m^3
(10) Lower Plenum Fluid Volume	1.38	m^3
(11) Steam Generator Inlet Plenum Simulator Flow Area	0.626	m^2
(12) Steam Generator Inlet Plenum Simulator Fluid Volume	0.931	m^3
(13) Steam Water Separator Fluid Volume	5.3	m^3
(14) Flow Area at the Top Plate of Steam Generator Inlet Plenum Simulator	0.195	m^2
(15) Hot Leg Flow Area	0.0826	m^2

* Flow area in the core is 0.35 m^2, including the excess flow area of gaps between the bundle and surface of thermal insulator and between the core barrel and the pressure vessel wall.

(Continued)

(16)	Intact Cold Leg Flow Area (Diameter = 297.9 mm)	0.0697 m^2
(17)	Broken Cold Leg Flow Area (Diameter = 151.0 mm)	0.0179 m^2
(18)	Containment Tank I Fluid Volume	30 m^3
(19)	Containment Tank II Fluid Volume	50 m^3

3. Elevation & Height

(1)	Top Surface of Upper Core Support Plate (UCSP)	0 mm
(2)	Bottom Surface of UCSP	- 76 mm
(3)	Top of the Effective Heated Length of Heater Rod	- 393 mm
(4)	Bottom of the Skirt in the Lower Plenum	-5270 mm
(5)	Bottom of Intact Cold Leg	+ 724 mm
(6)	Bottom of Hot Leg	+1050 mm
(7)	Top of Upper Plenum	+2200 mm
(8)	Bottom of Steam Generator Inlet Plenum Simulator	+1933 mm
(9)	Centerline of Loop Seal Bottom	-2281 mm
(10)	Bottom Surface of End Box	- 185.1mm
(11)	Top of the Upper Annulus	+2234 mm
(12)	Height of Steam Generator Inlet Plenum Simulator	1595 mm
(13)	Height of Loop Seal	3140 mm
(14)	Inner Height of Hot Leg Pipe	737 mm
(15)	Bottom of Lower Plenum	-5770 mm
(16)	Top of Upper Head	+2887 mm

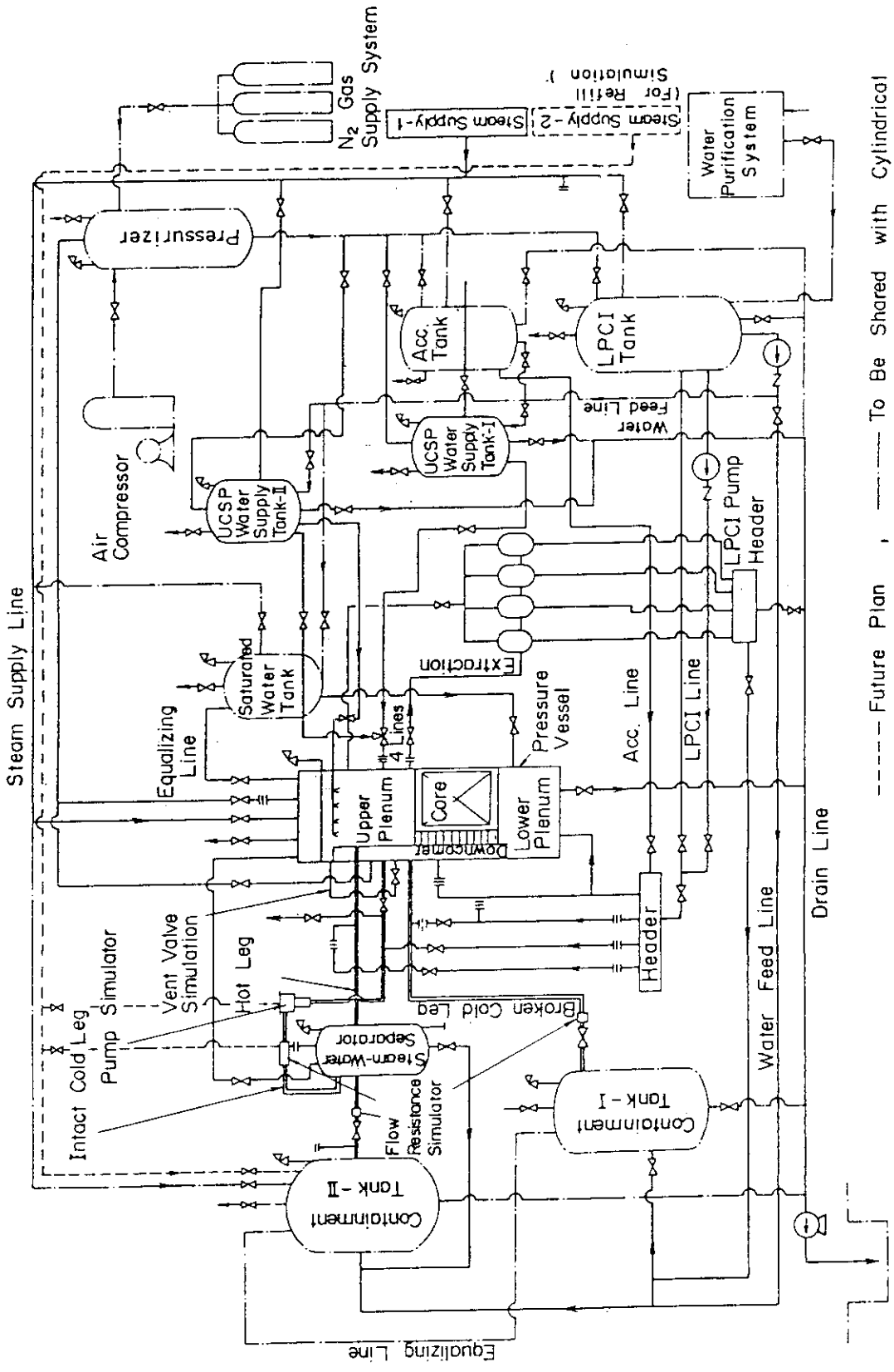

Fig.A-1 Schematic diagram of SCTF

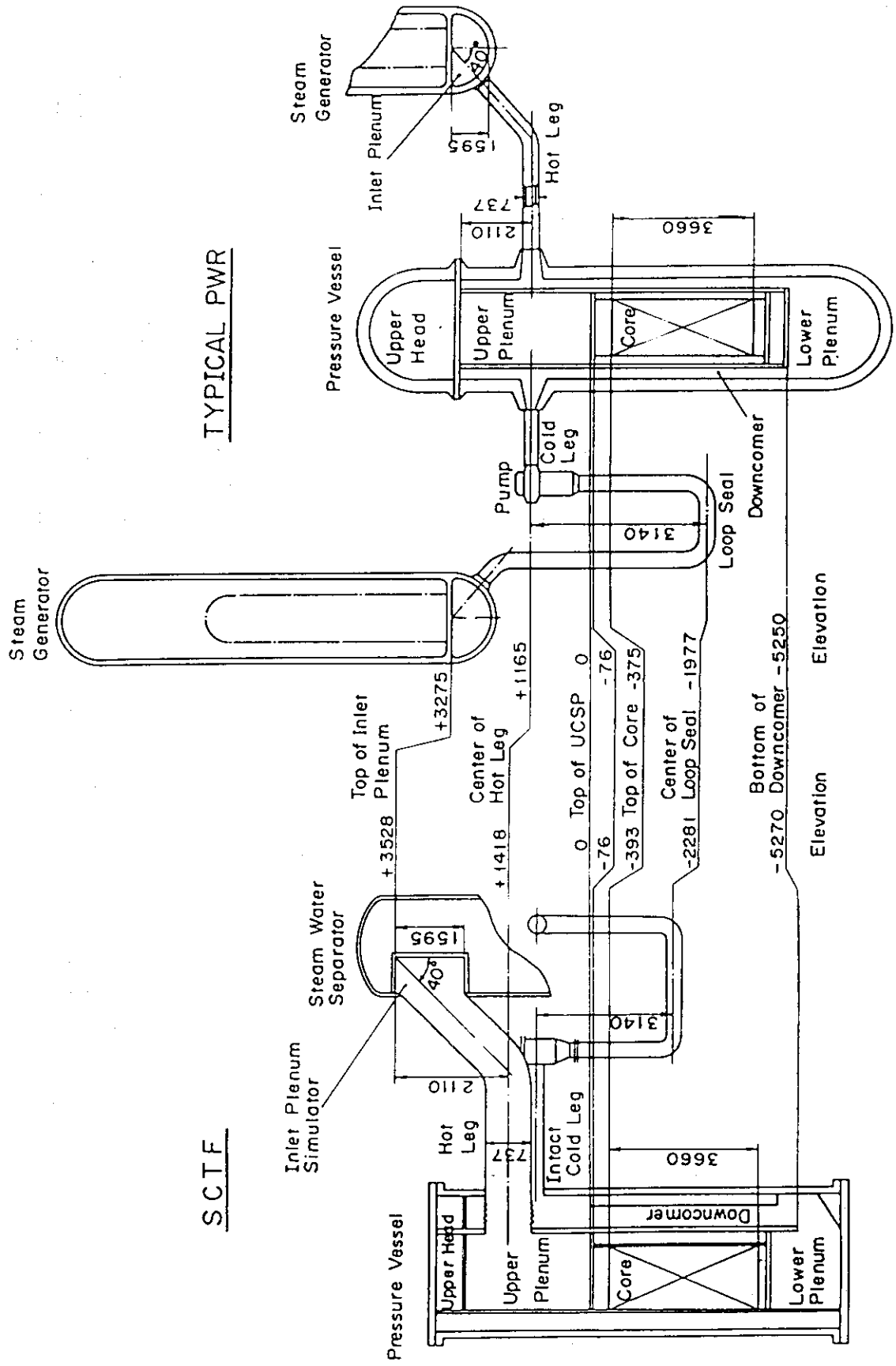

Fig.A-2 Comparison of SCTF and typical PWR

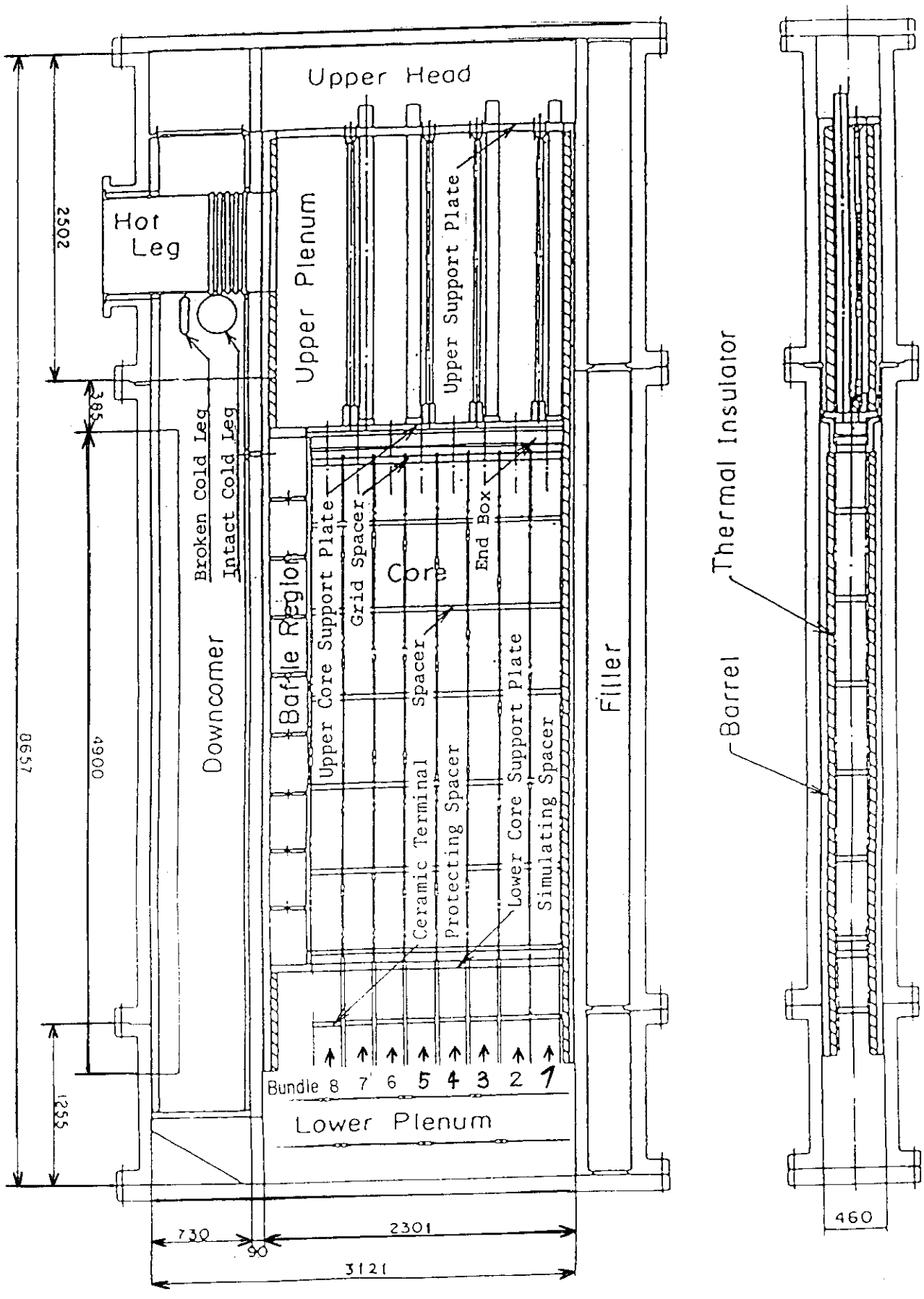

Fig.A-3 Schematic diagram of SCTF pressure vessel